Lebanese American University Repository (LAUR)

Post-print version/Author Accepted Manuscript

Publication metadata

Title: Fast and reduced full-system finite element solution of elastohydrodynamic lubrication problems: Line contacts.

Author(s): W. Habchi, J. Issa

Journal: Advances in Engineering Software

DOI/Link: https://doi.org/10.1016/j.advengsoft.2012.11.009

How to cite this post-print from LAUR:

Habchi, W., & Issa, J. (2013). Fast and reduced full-system finite element solution of

elastohydrodynamic lubrication problems: Line contacts. Advances in Engineering Software,

DOI: 10.1016/j.advengsoft.2012.11.009, URI: http://hdl.handle.net/10725/2179

  ⓒ Year 2013

This paper is posted at LAU Repository

For more information, please contact: archives@lau.edu.lb

Fast and Reduced Full-System Finite Element Solution of Elastohydrodynamic Lubrication Problems: Line Contacts

W. Habchi and J. Issa

Lebanese American University, Department of Industrial and Mechanical Engineering, Byblos, Lebanon

Abstract:

This paper presents a reduced full-system finite element solution of elastohydrodynamic lubrication (EHL) problems. It aims to demonstrate the feasibility of this approach by applying it to the simple isothermal Newtonian line contact case. However the proposed model can be extended to more complex situations. This model is based on a full-system finite element resolution of the EHL equations: Reynolds, linear elasticity and load balance. A reduced model is proposed for the linear elasticity problem. For this, three different techniques are tested: the classical "modal reduction" and "Ritz-vector" methods and a novel "EHL-basis" method. The reduction order in the first two appears to be insufficient and a large number of degrees of freedom is required in order to attain an acceptable solution. On the other hand, the "EHL-basis" method shows up to be much more efficient, requiring only a few degrees of freedom to compose the elastic deformation of the solid components. In addition, a comparison with the full model shows an order of magnitude execution time gain with errors of the order of only 1‰ for the central and minimum film thicknesses.

Keywords: Elastohydrodynamic Lubrication, Finite Elements, Model Reduction, Full-System Approach.

1. Introduction

Lubrication has been a topic of interest for the engineering community during the last century. In particular, Elastohydrodynamic lubrication (EHL) has gained much attention since its recognition as the main physical mechanism behind the successful operation of important mechanical elements such as roller bearings and transmission gears. Numerical modeling of this lubrication regime has always faced major difficulties mostly related to the high dependence of common lubricants viscosities on pressure and the relatively large elastic deformations of the contacting elements. In fact, these contacts can be subject to very high pressures that can reach several GPa and the film thicknesses involved can go down to a few nanometers. These difficulties have lead throughout the years to the introduction of different numerical approaches with one aim which is to have a robust and fast EHL solver that would cover a large range of operating conditions. All these approaches fall within two major categories: Semi-System and Full-System. In the first, the different EHL equations are solved separately and an iterative procedure is established between their respective solutions. The weak coupling in these models leads to a loss of information that is compensated by underrelaxation, leading to slow convergence rates. Many examples of such models can be found in the literature. One of the first works using this approach was that of Dowson and Higginson [1] followed by the pioneering work of Hamrock and Dowson [2]. A major step forward was the introduction of multigrid techniques to EHL problems by Lubrecht et al. [3]. These techniques helped improve the convergence performance of the Semi-System approach and opened the way to solving EHL problems on small scale computers. In the Full-System approach, EHL equations are solved simultaneously, preventing any convergence degradation due to losses of information resulting from coupling. One of the first models to use such an approach is that of Rhode and Oh [4] who

solved the EHL problem (in a finite element framework) as one integro-differential equation using a Newton-Raphson procedure. Later on, a similar work was provided by Houpert and Hamrock [5]. More recently, Hughes et al. [6] used the differential deflection method [7] in order to solve the EHL problem using the finite element method within a Full-System framework. The list of references provided above is by no means an exhaustive one. A few milestone contributions have only been cited and the interested reader is referred to the references therein for a more exhaustive coverage of the literature.

Although the Full-System based models mentioned above provide some attractive convergence properties, these have always suffered from three major drawbacks. First, the tedious implementation of the cavitation condition because of the simultaneous solution of all pressure updates. Second, the elastic deflection calculation in these models is based on a half-space approach. Therefore, the elastic deflection at any discretization point is related to all other points of the computational domain by means of the integral calculation. This results in a full Jacobian matrix that requires an important computational overhead in order to invert it. Finally, for heavily loaded contacts, the Jacobian matrix becomes almost singular which makes the solution hard to reach. In a recent work, Habchi et al. [8-10] introduced a finite element Full-System approach where the elastic deflection calculation was based on a linear elasticity model. This lead to a sparse Jacobian matrix since every discretization point belonging to a certain number of finite elements is only connected to its neighbouring points belonging to these elements. Thus the problem of the large computational overhead associated to the inversion of a full Jacobian matrix was overcome. However, a significantly larger, but sparse, Jacobian matrix is obtained resulting in reduced computational overhead associated with its inversion. In addition, the authors used a penalty method as proposed by Wu [11] to deal with the free boundary problem.

This method is implemented in a straightforward manner, by adding an additional penalty term to the Reynolds' [12] equation. Finally, special stabilized finite element formulations were introduced for the solution of highly loaded contacts. Hence, all difficulties associated so far to the Full-System approach were overcome, allowing this model to take full advantage of its fast convergence properties. In addition, this model was shown to have the same complexity as state of the art ones, but faster convergence rates. This is only true up to a certain problem size since the complexity of the employed sparse direct solver slightly exceeds $O(n)$ for large n values (where n is the total number of unknowns in the problem). This restriction can be alleviated by the use of iterative solvers as proposed in [13] where an EHL solver with $O(n)$ complexity is developed, for linear finite elements, based on a multigrid preconditioned GMRES iterative linear solver. It is worth noting that even with an algorithm of $O(n)$ complexity, the complexity of the Full-System approach is only the same as state of the art ones provided the number of linear elasticity unknowns can be bounded by $n_p \log(n_p)$ where n_p is the number of pressure unknowns in the problem. This is entirely possible with the use of locally refined meshes as is the case with the Full-System approach. Finally, the use of the finite element method which enables non-regular non-structured meshing lead to smaller size systems and hence faster solutions.

Although the model discussed above provides interesting performance properties compared to existing ones, a major improvement is possible and highly desirable to tackle computationally demanding problems (e.g. point contacts, transient EHL problems). In fact, as stated earlier, the elastic deflection of the solid elements is computed by means of a linear elasticity approach. The latter is applied to the entire solid domain, whereas for the EHL solution, only the surface deflection in the contact area is needed. Hence, a large number of degrees of freedom (dof) that

is being computed is not useful in practice. The aim of this paper is to improve the elastic deflection calculation by reducing the size of the corresponding model. Several techniques can be found in the literature for reducing the size of linear elasticity problems e.g. Boundary Element Method (BEM) [14], Infinite Elements [15], Model Order reduction [16]. However, the BEM method leads to full matrix systems and Infinite Elements have to be used in regions away from the contact area where the mesh size is usually relatively large and therefore the reduction in the size of the overall matrix system is relatively small. Hence, this work will focus on investigating the possibility of applying Model Order Reduction techniques to the EHL problem. Therefore, line contacts operating under steady-state regime shall be considered. Although the solution of line contact problems is relatively fast without the need for any model reduction techniques, it is important to explore the proposed method on the simple case before moving on to the more complicated, more computationally demanding cases. Besides, the method introduced in the following is not restricted to the simple line contact case and can be extended to more general applications. In the following, the lubricant is assumed to have a Newtonian behavior, thermal effects are neglected, and solid surfaces are taken to be smooth.

2. EHL theory and equations

Line contacts take place between two solid elements having an infinite radius of curvature in one of the principal space directions (*y*-direction). Such contacts can be reduced to an equivalent contact between a cylinder and a flat surface with the cylinder having an equivalent radius of curvature R in the *x*-direction as shown in Figure 1. The surfaces of these elements are pressed against each other by an external applied force F, they are separated by a full lubricant film and have constant unidirectional surface velocities in the *x*-direction.
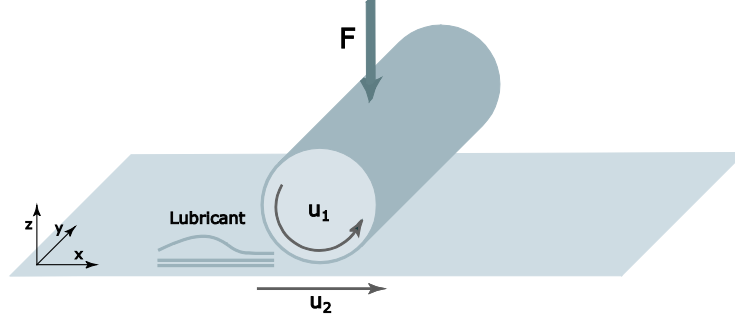
Figure 1: Geometrical description of a line contact

Three main equations define an EHL problem: the Reynolds equation which describes the pressure distribution p in the contact area, the linear elasticity equations which determine the elastic deformation of the contacting elements and the load balance equation which ensures that the correct load F is applied. All equations are written in dimensionless form using the Hertzian dry contact parameters [17] (i.e. Hertzian contact pressure p_h and Hertzian contact half-width a). The Reynolds [12] equation describing the dimensionless pressure distribution P for a steady-state line contact problem with unidirectional surface velocities u_1 and u_2 in the X-direction is given by:

$$\frac{\partial}{\partial X} \cdot \left(\varepsilon \frac{\partial P}{\partial X} \right) - \frac{\partial \left(\bar{\rho} H \right)}{\partial X} = 0 \tag{1}$$

Where: $\varepsilon = \dfrac{\bar{\rho} H^3}{\bar{\mu} \lambda}$, $\quad \lambda = \dfrac{12 u_m \mu_R R^2}{a^3 p_h}$ $\quad$ and $\quad u_m = \dfrac{u_1 + u_2}{2}$

This equation stems from the Navier-Stokes equations to which the thin film simplifying assumptions are applied. H is the film thickness. The dimensionless viscosity $\bar{\mu}$ and density $\bar{\rho}$ vary with pressure throughout the contact domain Ω_c (See Figure 2) making the problem highly nonlinear.
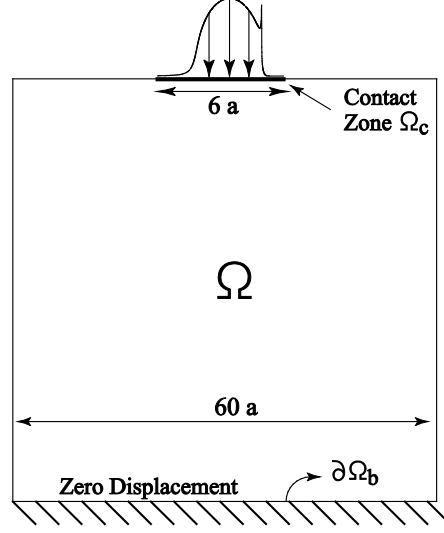
Figure 2: Computational domain of the line contact problem

The modified WLF model proposed by Yasutomi et al. [18] is used for viscosity variations with respect to pressure:

$$\mu(p) = \mu_g \times 10^{\frac{-C_1 \cdot (T_0 - T_g(p)) \cdot F(p)}{C_2 + (T_0 - T_g(p)) \cdot F(p)}}$$

(2)

$$\text{with: } T_g(p) = T_g(0) + A_1 \ln(1 + A_2 p)$$
$$F(p) = 1 - B_1 \ln(1 + B_2 p)$$

Where T_0 is the ambient temperature. As for density variations with pressure, the Dowson and Higginson [19] model is used:

$$\rho(p) = \rho_R \left[1 + \frac{0.6 \times 10^{-9} p}{1 + 1.7 \times 10^{-9} p} \right]$$

(3)

Neglecting body loads, the linear elasticity equations consist in finding the displacement vector $U = \{u, v\}$ over the *2D* computational domain Ω such that:

$$div(\sigma) = 0 \ \ with \ \ \sigma = C \ \varepsilon_s(U)$$

(4)

7

Where σ is the stress tensor, ε_s the strain tensor and C the compliance matrix. Line contacts being infinitely long in the y-direction, a plane-strain approximation is assumed. The computational domain Ω of the linear elasticity problem is a square which edges are large enough compared to the contact area (See Figure 2) in order to satisfy the half-space approximation and avoid any side effects. An edge length of at least $60a$ was shown to be sufficient [8]. In order to simplify the computational model, an equivalent problem is defined to replace the elastic deformation computation for both contacting bodies under the same pressure distribution. The equivalent model is defined by applying eq. (4) to a body that has the following material properties [9]:

$$E_{eq} = \frac{E_1^2 E_2 \left(1+\upsilon_2\right)^2 + E_2^2 E_1 \left(1+\upsilon_1\right)^2}{\left[E_1\left(1+\upsilon_2\right) + E_2\left(1+\upsilon_1\right)\right]^2} \quad \text{and} \quad \upsilon_{eq} = \frac{E_1\upsilon_2\left(1+\upsilon_2\right) + E_2\upsilon_1\left(1+\upsilon_1\right)}{E_1\left(1+\upsilon_2\right) + E_2\left(1+\upsilon_1\right)} \tag{5}$$

Moreover, by multiplying the equivalent Young's Modulus by a/R the dimensionless displacement vector is obtained directly and dividing it by p_h allows the use of the dimensionless pressure distribution P as a pressure load in the contact area. Hence, the equivalent material properties become:

$$E_{eq} = \frac{E_1^2 E_2 \left(1+\upsilon_2\right)^2 + E_2^2 E_1 \left(1+\upsilon_1\right)^2}{\left[E_1\left(1+\upsilon_2\right) + E_2\left(1+\upsilon_1\right)\right]^2} \times \frac{a}{R\, p_h} \quad \text{and} \quad \upsilon_{eq} = \frac{E_1\upsilon_2\left(1+\upsilon_2\right) + E_2\upsilon_1\left(1+\upsilon_1\right)}{E_1\left(1+\upsilon_2\right) + E_2\left(1+\upsilon_1\right)} \tag{6}$$

The previous simplification is equivalent to considering that one of the bodies is rigid while the other (that has the equivalent material properties defined in eq. (6)) accommodates the total elastic deflection of both surfaces. This avoids running a similar calculation twice (once for each solid body).

The film thickness H contains three contributions: the rigid body separation H_0, the original undeformed geometrical shape and the elastic deflection of the solid components δ:

8

$$H(X) = H_0 + \frac{X^2}{2} + \delta(X) \quad \text{with} \quad \delta(X) = |v(X)| \tag{7}$$

Where $v(X)$ corresponds to the elastic displacement in the z-direction. Finally, the load balance equation is written in dimensionless form as follows:

$$\int_{\Omega_c} P(X) dX = \frac{\pi}{2} \tag{8}$$

Where $\pi/2$ corresponds to the dimensionless external load. This equation ensures that the correct external load F is applied. The latter is controlled by the value of the film thickness constant H_0.

To complete these equations, boundary conditions must be supplied for Reynolds' and the linear elasticity equations. For Reynolds' equation, the pressure is considered to be zero at the boundaries of the contact area:

$$P = 0 \quad \text{on} \ \partial\Omega_c \tag{9}$$

As for the complementary film rupture boundary condition, which is used to define the free exit boundary of the contact:

$$P \geq 0 \quad \text{on} \ \Omega_c \ \text{and} \ P = \nabla P \cdot \vec{n}_c = 0 \ \text{on the cavitation boundary} \tag{10}$$

Where $\vec{n}_c$ is the outward normal vector to the outlet boundary of the contact. Finally, the boundary conditions of the elastic problem are defined as follows:

$$\begin{cases} U = 0 & \text{at the bottom boundary } \partial\Omega_b \\ \sigma_n = \sigma \cdot \vec{n} = -P & \text{at the contact area boundary } \Omega_c \\ \sigma_n = 0 & \text{elsewhere} \end{cases} \tag{11}$$

These boundary conditions along with the different EHL equations provided above completely define the mathematical model used to describe the behaviour of smooth isothermal Newtonian EHL line contacts operating under steady-state regime.

3. Full and Reduced Models

The full model for line contact problems has been previously introduced in [8-10] and in this section only a brief reminder of this model shall be provided. On the other hand, the reduced model, which constitutes the core of this paper, shall be described into more detail. Both models are based on the Full-System finite element approach introduced in [8-10]. The three EHL equations (Reynolds, elasticity and load balance) are solved simultaneously using a damped Newton procedure as described in [20]. The free boundary problem is treated by means of a penalty method as proposed by Wu [11]. The latter consists in adding a penalty term to the Reynolds equation. This term acts only in the negative pressure region and forces the negative pressures towards zero. Reynolds equation thus becomes:

$$\frac{\partial}{\partial X} \cdot \left(\varepsilon \frac{\partial P}{\partial X} \right) - \frac{\partial(\bar{\rho}H)}{\partial X} - \xi \cdot P^- = 0 \qquad (12)$$

Where ξ is an arbitrary large positive number and $P^- = \min(P,0)$ corresponds to the negative part of the pressure distribution. In addition, for heavily loaded contacts, the Galerkin Least Squares (GLS) finite element formulation introduced in [10] is used.

3.1 Full Model

In the full model, the linear elasticity equations (4) are applied to the entire solid geometrical domain Ω, whereas Reynolds' equation is applied only to the one-dimensional contact area Ω_c. On the other hand, the load balance equation is an ordinary integral equation that is added

directly to the system of equations formed by the Reynolds and linear elasticity equations, along with the introduction of an additional unknown H_0. The weak form finite element formulation of the obtained system of equations reads:

Find $(U, P, H_0) \in S_U \times S_P \times R$ such that $\forall (W_U, W_P, W_{H_0}) \in S_U \times S_P \times R$, one has:

$$
\begin{cases}
\int_\Omega -C\varepsilon_s(U) \cdot \varepsilon_s(W_U) d\Omega + \int_{\Omega_c} -P \cdot \vec{n}\ W_U\ d\Omega = 0 \\[2mm]
\int_{\Omega_c} -\varepsilon \frac{\partial P}{\partial X} \frac{\partial W_P}{\partial X} d\Omega + \int_{\Omega_c} \overline{\rho} H \frac{\partial W_P}{\partial X} d\Omega - \int_{\Omega_c} \xi \cdot P^- W_P\ d\Omega = 0 \\[2mm]
\int_{\Omega_c} P W_{H_0} d\Omega - \frac{\pi}{2} W_{H_0} = 0
\end{cases}
\tag{13}
$$

Where: $S_U = \left\{ U \in H^1(\Omega) \times H^1(\Omega) / U = 0 \text{ on } \partial\Omega_b \right\}$ and $S_P = \left\{ P \in H^1(\Omega_c) / P = 0 \text{ on } \partial\Omega_c \right\}$

Let us now write the discrete form of the previous system of equations. Consider $\Omega^h = \{\Omega_1, \dots, \Omega_{n_e}\}$ a finite element partition of Ω such that: $\overline{\Omega} = \cup_{e=1}^{n_e} \overline{\Omega}_e$, $\overline{\Omega} = \Omega \cup \partial\Omega$, $\overline{\Omega}_e = \Omega_e \cup \partial\Omega_e$ and $\Omega_e \cap \Omega_{e'} = \phi$ if $e \neq e'$. n_e denotes the total number of elements in the partition while $\partial\Omega$ and $\partial\Omega_e$ denote respectively the boundaries of the domain Ω and the element Ω_e. Let Ω_{ce} be the set of elements representing the *1D* contact domain Ω_c and defined by $\Omega_{ce} = \{\Omega_e \cap \Omega_c / \Omega_{ce} \neq \varnothing\}$ and let n_{ce} be the total number of elements belonging to Ω_{ce}. Let $S_U^h \subset S_U$ and $S_P^h \subset S_P$. The discrete functions U^h and P^h defining these spaces have the same characteristics as their analytical equivalents U and P defined above with the only difference that $U^h \in L^l$ and $P^h \in L^l$ where L^l is the set of interpolation polynomials of degree equal to l defined within each element Ω_e. The discrete form of the previous system of equations is

11

obtained by replacing the field variables U and P by their discrete equivalents $U^{h^{(e)}}$ and $P^{h^{(e)}}$ within every discretization element e:

$$U^{h^{(e)}} = \sum_{i=1}^{n_U} U_i^{(e)} N_{Ui} \quad \text{and} \quad P^{h^{(e)}} = \sum_{i=1}^{n_P} P_i^{(e)} N_{Pi} \tag{14}$$

Where $U_i^{(e)}$ and $P_i^{(e)}$ are the nodal values of U and P respectively, associated to the interpolation functions N_{Ui} and N_{Pi} within the element e (n_U and n_P being their respective numbers). Similarly, the weighting functions W_U and W_P are approximated by $W_U^{h^{(e)}}$ and $W_P^{h^{(e)}}$ respectively:

$$W_U^{h^{(e)}} = \sum_{i=1}^{n_U} W_{Ui}^{(e)} N_{Ui} \quad \text{and} \quad W_P^{h^{(e)}} = \sum_{i=1}^{n_P} W_{Pi}^{(e)} N_{Pi} \tag{15}$$

Where $W_{U,i}^{(e)}$ and $W_{P,i}^{(e)}$ are the nodal values of the weight functions W_U and W_P within the element e respectively. Finally, by adding the stabilizing GLS term to Reynolds equation, the discrete form of the system of equations (13) becomes:

Find $\left(U^h, P^h, H_0\right) \in S_U^h \times S_P^h \times R$ such that $\forall \left(W_U^h, W_P^h, W_{H_0}\right) \in S_U^h \times S_P^h \times R$, one has:

$$
\begin{cases}
\displaystyle\int_{\Omega^h} -C\varepsilon_s\left(U^h\right) \cdot \varepsilon_s\left(W_U^h\right) d\Omega + \int_{\Omega_c^h} -P^h \cdot \vec{n}\, W_U^h d\Omega = 0 \\[2em]
\displaystyle\int_{\Omega_c^h} -\varepsilon \frac{\partial P^h}{\partial X} \frac{\partial W_P^h}{\partial X} d\Omega + \int_{\Omega_c^h} \overline{\rho} H \frac{\partial W_P^h}{\partial X} d\Omega \overbrace{- \int_{\Omega_c^h} \xi \cdot P^{h-} W_P^h d\Omega}^{Penalty\ term} \\[2em]
\qquad\qquad \underbrace{- \sum_{e=1}^{n_{ce}} \int_{\Omega_{ce}} R_h\left(P^h\right) \tau \left(H \frac{\partial \overline{\rho}}{\partial P} \frac{\partial W_P^h}{\partial X} - \frac{\partial}{\partial X}\left(\varepsilon \frac{\partial W_P^h}{\partial X}\right)\right) d\Omega = 0}_{GLS\ term} \\[2em]
\displaystyle\int_{\Omega_c^h} P^h W_{H_0} d\Omega - \frac{\pi}{2} W_{H_0} = 0
\end{cases}
\tag{16}
$$

Where R_h is the residual of the hydrodynamic problem (Reynolds equation). The tuning parameter τ is defined as:

12

$$\tau = \frac{h_e}{2|\beta|l}\xi(Pe)$$

$$\text{with: } \beta = H\frac{\partial\overline{\rho}}{\partial P}, \quad Pe = \frac{|\beta|h_e}{2\overline{\varepsilon}\,l} \quad \text{and} \quad \xi(Pe) = \coth(Pe) - \frac{1}{Pe}$$

(17)

Where h_e and Pe are respectively the characteristic length and the local Peclet number of the element e. l is the polynomial order of the hydrodynamic problem's Lagrange shape functions N_P. In the current work, second order Lagrange elements ($l = 2$) are employed for both the elastic and hydrodynamic problems (N_U and N_P). The system of equations (16) is nonlinear and a Damped-Newton [20] procedure is employed in order to solve it. The latter gives rise to a linearized system of equations (as a function of the increments δU, δP and δH_0) to solve at every Newton iteration i:

$$\begin{bmatrix} K_{ee} & K_{eh} & \varnothing \\ K_{he} & K_{hh} & K_{hl} \\ \varnothing & K_{lh} & \varnothing \end{bmatrix}^{i-1} \begin{Bmatrix} \delta U \\ \delta P \\ \delta H_0 \end{Bmatrix}^{i} = \begin{Bmatrix} R_e \\ R_h \\ R_l \end{Bmatrix}^{i-1}$$

(18)

The subscripts e, h and l stand for "elastic", "hydrodynamic" and "load balance" respectively. N_{2D} is the number of nodes in the *2D* mesh associated to the elastic problem whereas N_{1D} is the number of nodes in the *1D* mesh associated to the hydrodynamic problem. Hence, the total number of unknowns or dof of the elastic problem is $2 \times N_{2D}$ since 2 dof are associated to every node. These are δu and δv, the increments of the elastic deflections in the x and z directions respectively. On the other hand, the total number of unknowns of the hydrodynamic problem is

13

N_{1D} since 1 dof (δP) is associated to each node. The total number of unknowns is then defined as:

$$N_{dof} = 2 \times N_{2D} + N_{1D} + 1 \tag{19}$$

The matrix on the left-hand-side is the Jacobian matrix whereas the right-hand-side vector is formed by the residual vectors of the elastic, hydrodynamic and load balance equations (R_e, R_h and R_l respectively). Starting with an initial guess of the solution (Hertzian pressure distribution and its corresponding elastic deflection), the system of equations (18) is solved at every Newton iteration i using a direct linear system solver (UMFPACK [21]). The result is added to the solution obtained at the previous iteration according to:

$$\left\{ \begin{matrix} U \\ P \\ H_0 \end{matrix} \right\}^{i} = \left\{ \begin{matrix} U \\ P \\ H_0 \end{matrix} \right\}^{i-1} + \lambda_i \left\{ \begin{matrix} \delta U \\ \delta P \\ \delta H_0 \end{matrix} \right\}^{i} \tag{20}$$

Where $\lambda_i \in [0,1]$ is a "damping factor" computed according to [20]. This operation is repeated until convergence of the solution is obtained. The convergence criteria are also provided in [20].

Remark: Note that the elastic problem and the load balance equation are linear. Hence, their corresponding contributions to the Jacobian matrix K_{ee}, K_{eh} and K_{lh} remain unchanged throughout the nonlinear resolution procedure. These matrices are only assembled once (at the 1st iteration), and the result is used throughout the iterative procedure.

3.2 Reduced Model

Although the model described above has been shown to have the same complexity as state of the art EHL solvers with faster convergence rates and smaller size systems, leading to smaller

execution times (the interested reader is referred to [8-10]), a major improvement is yet to be achieved. In fact, the elastic problem is solved over the sufficiently large two-dimensional geometrical domain associated to the solid elements. However, in practice, only the elastic deflection in the one-dimensional contact area Ω_c is needed for the EHL solution. Hence, a large number of dof is being computed in vain. The idea here is to make the elastic calculation more efficient by reducing the size of its corresponding model.

The reduced model is obtained by a simple change of solution space. In fact, the finite element formulation (15) remains the same with the only difference that the solution space S_U for the elastic problem is now replaced by a reduced "richer" one $\tilde{S}_U$. The latter has the same properties as S_U, but is formed by a smaller set of functions. However, these functions are now defined over the entire two-dimensional geometrical domain Ω, contrarily to those forming S_U which, for a given element Ω_e, are only defined inside the element and take a value of zero elsewhere. This property is the main reason behind the richness of $\tilde{S}_U$ compared to S_U. Let N_m be the total number of functions φ^i ($i=1, 2, \ldots, N_m$) forming $\tilde{S}_U$. From this point on, these functions are referred to as "basis functions" and the vectors describing their discrete form over the two-dimensional mesh of the elastic problem are referred to as "basis vectors". Now, the elastic deflection U can be formed as a linear combination of the basis functions:

$$U = \sum_{i=1}^{N_m} \alpha_i \, \varphi^i \tag{21}$$

Where the parameters α_i are known as "Generalized Coordinates". Equation (21) can be written in discrete form (within an element e) as:

$$U^{h^{(e)}} = \sum_{i=1}^{N_m} \alpha_i \, \varphi^{i,h^{(e)}} \tag{22}$$

Where $\varphi^{i,h^{(e)}}$ is the discrete equivalent of φ^i defined over the element e as:

$$\varphi^{i,h^{(e)}} = \sum_{j=1}^{n_U} \varphi_j^{i^{(e)}} \, N_{Uj} \tag{23}$$

Where $\varphi_j^{i^{(e)}}$ ($j = 1 \ldots n_U$) are the nodal values of φ^i within element e. Hence, the reduced discrete

system of equations is now obtained by replacing U, P, W_U and W_P by their discrete equivalents

$U^{h^{(e)}}$ (given by eq. (22)), $P^{h^{(e)}}$, $W_U^{h^{(e)}}$ and $W_P^{h^{(e)}}$. However, in contrast with the full model case,

$U^{h^{(e)}}$ and $W_U^{h^{(e)}}$ belong now to $\tilde{S}_U^h$ instead of S_U^h. The unknowns of the elastic problem are now

the generalized coordinates α_i. Their number is N_m compared to $2 \times N_{2D}$ in the full model case.

And the matrix form of the linearized system of equations to solve at every Newton iteration i

now becomes:

$$\overset{N_m \quad\quad N_{1D} \quad 1}{\begin{matrix} N_m \\ \\ N_{1D} \\ \\ 1 \end{matrix} \begin{bmatrix} \tilde{K}_{ee} & \tilde{K}_{eh} & \varnothing \\ \tilde{K}_{he} & K_{hh} & K_{hl} \\ \varnothing & K_{lh} & \varnothing \end{bmatrix}^{i-1} \begin{Bmatrix} \delta\alpha \\ \delta P \\ \delta H_0 \end{Bmatrix}^{i} = \begin{Bmatrix} \tilde{R}_e \\ R_h \\ R_l \end{Bmatrix}^{i-1}} \tag{24}$$

With: $\tilde{K}_{ee} = \Phi^T K_{ee} \Phi$, $\tilde{K}_{eh} = \Phi^T K_{eh}$ and $\tilde{K}_{he} = K_{he} \Phi$

$\tilde{R}_e$ is the residual of the reduced elastic problem whereas Φ is the $2N_{2D} \times N_m$ transformation

matrix which columns correspond to the basis vectors.

Remark: Note that the reduced elastic problem remains linear, and therefore its corresponding contributions to the Jacobian matrix $\tilde{K}_{ee}$ and $\tilde{K}_{eh}$ are also assembled only at the 1st iteration of the nonlinear resolution procedure.

It is clear that the total number of dof of the reduced model is:

$$\tilde{N}_{dof} = N_m + N_{1D} + 1 \tag{25}$$

Hence, if one can define a sufficiently rich solution space $\tilde{S}_U$ such that the total number of basis functions required to reconstitute any EHL elastic deformation (within a wide range of operating conditions) $N_m << 2 \times N_{2D}$, then the size of the reduced model $\tilde{N}_{dof} << N_{dof}$. As a consequence, execution times are expected to be reduced.

Now that the basic principles behind the reduced model employed in this work have been introduced, the whole problem boils down to choosing an appropriate reduced solution space $\tilde{S}_U$. Model reduction of linear elasticity problems in itself is not a novel topic. In fact, numerous techniques can be found in the literature for the selection of the reduced solution space. The interested reader is referred to [22] and references therein for an exhaustive review of these techniques. In this work, three model reduction techniques are inspected. The first two are more or less classical: a "Modal Coordinate Reduction" technique also known as "Modal Reduction", which uses the mode shapes of a structure in order to form its reduced solution space and a "Ritz-vector-like" method which uses some load dependent deflections as basis vectors. Finally, the third method is a novel EHL-oriented one, which uses EHL deflections as basis vectors.

3.2.1 Modal Reduction Technique

Modal reduction is a classical model reduction technique that has been widely used in the literature [16]. The latter consists in using the mode shapes of a structure as basis functions.

These possess an interesting orthogonality property with respect to the stiffness matrix K_{ee}, making the reduced stiffness matrix $\tilde{K}_{ee}$ a diagonal matrix. The values of the diagonal terms are nothing else but the eigenvalues of the linear elasticity problem.

In order to test this method, a simple EHL case is considered. The values of the dimensionless Moes [23] parameters M and L are taken to be $M=30$ and $L=5$ respectively. The Hertzian contact pressure $p_h=0.46$GPa, and this contact is a lightly loaded one, which solution is normally easy to obtain using classical approaches. Figure 3 shows the dimensionless pressure and film thickness distributions obtained for this case by both the full and reduced models. The left hand figure clearly shows that for $N_m=100$ the dimensionless pressure profile exhibits an oscillatory behavior in the central area of the contact. Increasing the number of mode shapes to $N_m =1800$ (right) reduces the amplitude of these oscillations but does not completely remove them. In fact, the mode superposition technique defined in eq. (21) is known to generate micro-oscillations in the displacement field U [16]. In most linear elasticity applications, these oscillations are irrelevant and their effect is of minor importance. However, the EHL problem is very sensitive to these micro-oscillations in the elastic deflection. This is because under a wide range of operating conditions (especially in the high load regime) the elastic deflection of the solid components can be several orders of magnitude larger than the film thickness. Hence, any small error in the elastic deflection is amplified when included in the film thickness. Since the latter appears to the cubic power in the second order term of Reynolds equation, this effect is even further amplified and leads to important oscillations in the pressure distribution.
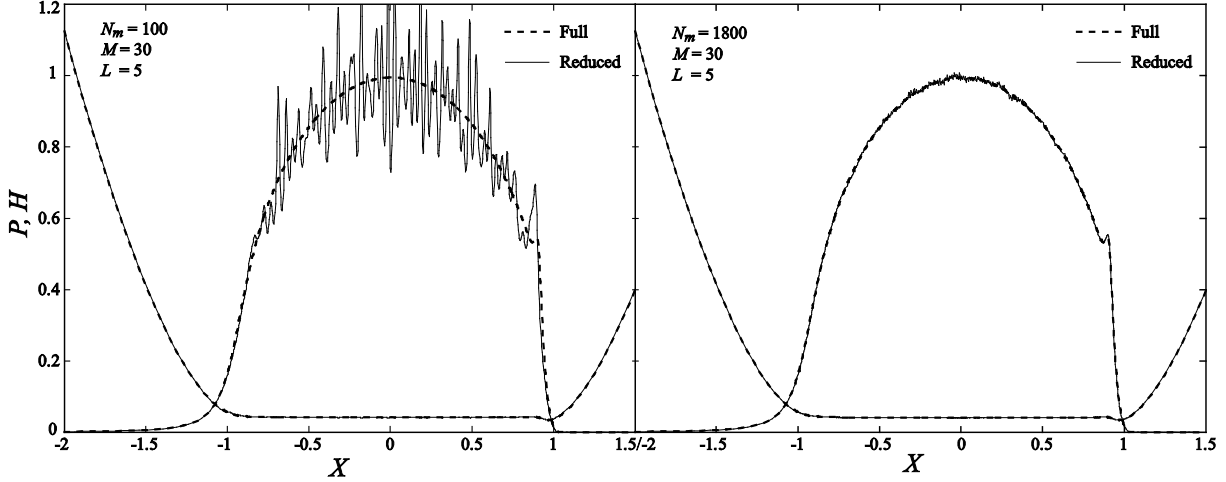
Figure 3: Dimensionless pressure and film thickness profiles obtained using the modal reduction technique for the case *M*=30, *L*=5 (p_h=0.46GPa) using 100 (left) and 1800 (right) mode shapes

It is clear that the results obtained by modal reduction in the simple case presented in Figure 3 are unsatisfactory, even when using a very large number of mode shapes (N_m=1800). For high loads, this spurious behavior is expected to be further amplified. Hence, a different, more stable alternative for the selection of the reduced solution space is to be investigated. Next, a Ritz-Vector-like method is discussed.

3.2.2 Ritz-Vector-like method

Ritz-vector methods are an attractive alternative for model reduction when a structure is subject to fixed spatial distribution of applied loads. This happens to be the case in EHL applications, where the external load is always a normal load applied over the contact area Ω_c. "Load Dependent Ritz Vectors" (LDRVs) are a particular and efficient class of Ritz vectors in which loading information on the structure is used to generate the vectors which form the reduced basis. Because Ritz vectors are created based on a specific load pattern, fewer vectors are typically needed to achieve the same level of accuracy as modal reduction techniques. The LDRV method was first proposed by Wilson et al. [24] and then improved by Nour-Omid and Clough [25][26].

These schemes employ static recurrence procedures to generate the LDRVs starting with a first vector that corresponds to the static deformation of the structure due to a particular applied pattern. The reduced basis formed by the LDRVs automatically satisfies the orthogonality property with respect to the stiffness matrix K_{ee}.

The same principle is employed in this section in order to develop a Ritz-Vector-like method, specifically designed for EHL applications. The first Ritz vector is generated by considering a Hertzian pressure distribution in the contact area whereas the remaining vectors are determined using the static recurrence procedure. In order to test this method, the same test case is considered as previously (M=30, L=5, p_h=0.46GPa). Figure 4 shows the dimensionless pressure and film thickness distributions obtained for this case by both the full and reduced models. The left hand side figure clearly shows that for N_m=100 the pressure distribution still exhibits an oscillatory behavior. However, note that the amplitude of these oscillations is smaller than that obtained using the modal reduction technique with the same number of basis vectors. Increasing the number of Ritz-Vectors N_m to 300 (right) reduces the amplitude of these oscillations to a much better extent than the case N_m=1800 using the modal reduction technique. But again, these oscillations are not completely smoothed out.
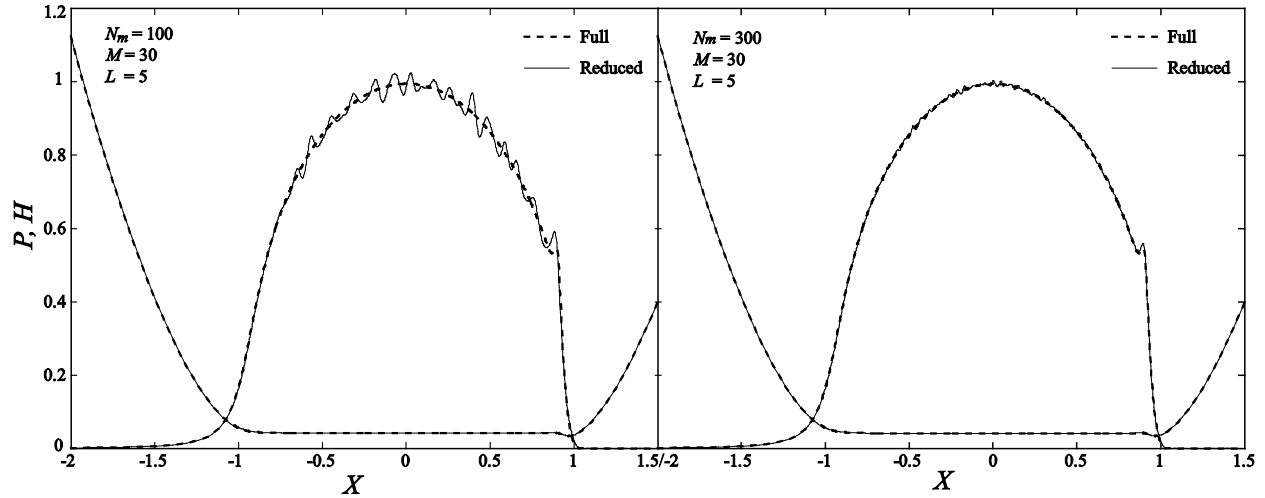
Figure 4: Dimensionless pressure and film thickness profiles obtained using the Ritz-Vector-like method for the case *M*=30, *L*=5 (p_h=0.46GPa) using 100 (left) and 300 (right) Ritz-Vectors

As expected, the Ritz-Vector-like method being load-dependent, it turned out to be more stable than the modal reduction technique. Yet, the number of Ritz-Vectors needed to reach an acceptable solution remains relatively high (N_m>300) for a relevant reduction in the computational effort to be obtained. This number is expected to be even higher for highly loaded cases. As a consequence, it seems unavoidable to consider a more EHL-oriented choice of the reduced solution space. This track is investigated next.

3.2.3 EHL-Basis Technique

Based on the unsatisfactory results obtained by the classical modal reduction and Ritz-vector like methods, it is unavoidable to adopt a more "EHL-oriented" strategy in the choice of basis functions for the reduced model. In this section, a novel method is proposed, where the basis functions are nothing else but EHL elastic deflections computed using the full model presented earlier. From this point on, the resulting basis is referred to as "EHL-basis". The corresponding functions are selected in such a way to cover a large range of operating conditions. The Moes

dimensionless load and material properties parameters, *M* and *L* respectively, are used to define this range. In fact, the EHL-basis functions are selected within a range of values $0 < M \leq 1000$ and $0 < L \leq 20$. Their selection is based on numerical experimentation and visualization of the corresponding deflections, mostly their deviation with respect to the Hertzian elastic deflection within the contact area Ω_c. The following observations were established:

1- It is important to distinguish three separate domains of operating conditions based on their values of *M*. These are $0 < M \leq 20$, $20 < M \leq 50$ and $50 < M \leq 1000$ corresponding to Low, Medium and High values of *M* respectively.

2- In the High *M* regime, often associated to high loads, the EHL solution is very sensitive to any micro-oscillations in the elastic deflection resulting from the superposition of a large number N_m of basis functions. This is because the elastic deflection in this regime is often several orders of magnitude larger than the film thickness. Hence, the slightest error in the elastic deflection has an important effect on the film thickness. In addition, since the latter appears to the cubic power in the second order term of Reynolds equation, this effect is even more amplified on pressure. As a consequence, a smaller and more scattered number of basis functions is to be employed under these conditions.

Based on the previous observations, three separate sets of basis functions were derived. These are shown in Figure 5 for the Low, Medium and High *M* regimes. For all three cases, the Hertzian elastic deflection is used as the first basis function. The remaining functions are marked by an x-tick in their corresponding grid showing their *M* and *L* values. The total number of basis functions N_m does not exceed 30 in all cases ($N_m = 29$ for Low and Medium *M* whereas $N_m = 22$ for high *M*). Note that for high *M*, the basis functions are more scattered and their number is reduced (relatively to the covered range of *M* and *L*) compared to the Low and Medium cases.

Finally, it is important to note that the choice of EHL-basis is not unique, however the one suggested in this work was found to provide stable solutions over the corresponding range of M and L.

<u>Remark:</u> Note that the EHL-basis functions are not orthogonal with respect to the linear elasticity stiffness matrix K_{ee}, leading to a full reduced stiffness matrix $\tilde{K}_{ee}$. However, considering their very small number ($N_m<30$), the total number of nonzero terms in $\tilde{K}_{ee}$ is negligible compared to K_{ee}.

Low M

L＼M	5	10	15	20
1	X	X	X	X
3	X	X	X	X
7	X	X	X	X
10	X	X	X	X
13	X	X	X	X
17	X	X	X	X
20	X	X	X	X

Medium M

L＼M	20	25	35	50
1	X	X	X	X
3	X	X	X	X
7	X	X	X	X
10	X	X	X	X
13	X	X	X	X
17	X	X	X	X
20	X	X	X	X

High M

L＼M	50	65	95	140	200	350	550	800	1000
1	X				X				X
2		X				X			
4			X				X		
7				X				X	
10	X				X				X
12		X				X			
14			X				X		
17				X				X	
20	X				X				X

*Hertizian elastic deflection is the first basis function in all three cases (Low, Medium and High M)

Figure 5: Composition of the EHL-basis for the Low (left), Medium (centre) and High M (right) regimes

In order to test this EHL-oriented method, three test cases are considered (one for each M regime). The first corresponds to $M=17$, $L=15$, $p_h=1.05$GPa (Low M), the second $M=30$, $L=5$, $p_h=0.46$GPa (Medium M) and finally $M=375$, $L=15$, $p_h=4.91$GPa (High M).

<u>Remark:</u> Note that for the last case considered, the Hertzian contact pressure $p_h=4.91$GPa is relatively high and may very rarely be encountered in real applications. Under such pressures, the solid materials may even be subject to plastic deformations and the linear elasticity approach

employed here is no longer valid. However, this case is considered here for the only purpose of showing the robustness of the proposed model.
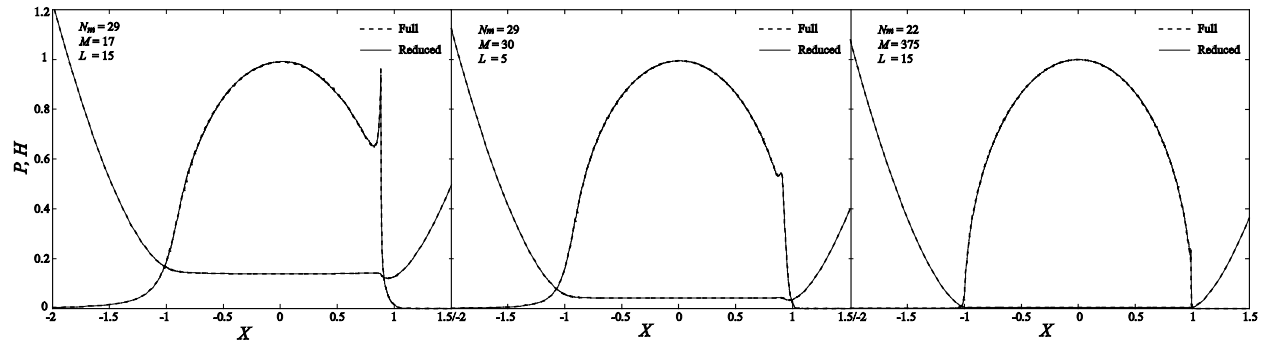

Figure 6: Dimensionless pressure and film thickness profiles obtained using the EHL-Basis method for 3 different test cases. Left: M=17, L=15, p_h=1.05GPa (Low M), Centre: M=30, L=5, p_h=0.46GPa (Medium M), Right: M=375, L=15, p_h=4.91GPa (High M)

Figure 6 shows the dimensionless pressure and film thickness distributions obtained by both the full and reduced models for the three test cases considered. It is clear that the solutions obtained by the reduced model perfectly match those obtained by the full one and no oscillations are observed. Hence, despite the relatively small number of basis functions employed in the EHL-Basis, the latter is rich enough to allow a robust and satisfactory solution of the problem. From this point on, only the EHL-Basis method is adopted and a thorough investigation of its numerical properties is realized.

4. Overall numerical procedure

In this section, the overall numerical procedure of the reduced model is described. The overall procedure consists of two main parts: Preprocessor and Solver. In the pre-processing phase, for a given mesh case, the mesh data is generated and stored on a text file. Then, the Full Model is employed to run Full calculations and generate the basis functions. For this, any typical lubricant can be used provided that the set of basis functions is derived for the M and L values indicated in

24

Figure 5. Then, these derived basis functions are stored on the same text file with the mesh data. Note that this pre-processing phase is carried out only once for a given mesh case and there is no need to regenerate the basis functions even for different lubricants (see following section). In the solver part, the first step is to read the mesh data along with the basis functions from the corresponding text file. Then, for a given set of operating conditions, the Reduced Model is employed to solve the different EHL equations using a damped Newton procedure as indicated in section 3.2.

5. Results

In the following, motivated by the promising results obtained using the EHL-Basis technique, a thorough investigation of the numerical performance of this method is presented. Five different mesh cases are considered in this section: "*Extra Coarse*", "*Coarse*", "*Normal*", "*Fine*" and "*Extra Fine*". Their respective properties are listed in Table 1 for both the full and reduced models.

Mesh Case	N_{2D}	N_{1D}	N_{dof}	$\tilde{N}_{dof}$	
				Low / Medium M	High M
Extra Coarse	741	105	1588	135	128
Coarse	1816	203	3836	233	226
Normal	5419	499	11338	529	522
Fine	10773	909	22456	939	932
Extra Fine	63927	4229	132084	4259	4252

Table 1: Properties of the different mesh cases considered

All mesh cases are developed such that the mesh size be fine in the Hertzian contact area, coarser in the inlet and outlet regions of the contact and even coarser and coarser with increasing distance from the *1D* contact area. This guarantees a custom-tailored "EHL-optimized" dof repartition over the *2D* computational domain *Ω*. Figure 7 shows the *"Extra Coarse"* (left), *"Normal"* (centre) and *"Extra Fine"* (right) mesh cases.
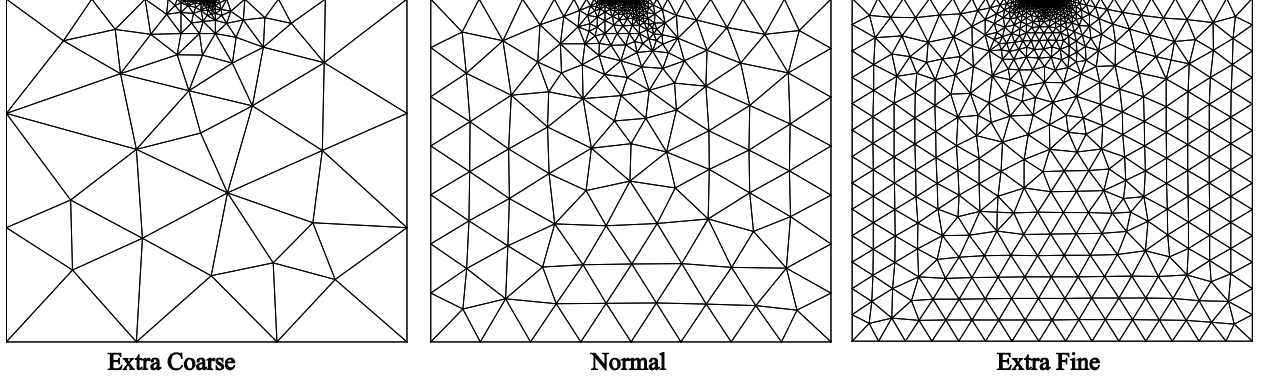
Figure 7: *"Extra Coarse"* (left), *"Normal"* (centre) and *"Extra Fine"* (right) mesh cases

In the following numerical tests, three different lubricants are considered: a standard paraffinic mineral base oil (CPRI), a low viscosity low pressure-viscosity mineral base oil (CPRP) and a synthetic hydrocarbon base lubricant of higher viscosity (PENNZ). Their modified WLF constant parameters are listed in Table 2 along with their ambient pressure viscosity μ_R and equivalent pressure-viscosity coefficient α^* also known as the reciprocal asymptotic isoviscous pressure coefficient [27] and defined as:

$$\alpha^* = \left[\int_0^\infty \frac{\mu(p=0)}{\mu(p)} dp \right]^{-1} \tag{26}$$

The modified WLF properties of the considered lubricants can be found in [28][29]. The ambient temperature is considered to be $T_0=25^{\circ}C$.

	WLF constant parameters								μ_R (Pa.s)	α^* (GPa^{-1})
	A_1(°C)	A_2(MPa^{-1})	B_1	B_2(MPa^{-1})	C_1	C_2(°C)	$T_g(0)$ (°C)	μ_g (Pa.s)		
CPRI	19.17	4.07x10^{-3}	0.230	0.0249	16.04	18.18	-73.86	10^{12}	0.02828	23.6
CPRP	22.47	4.22x10^{-3}	0.222	0.0349	15.87	10.22	-113.79	10^{12}	0.00165	12.5
PENNZ	69.81	1.68x10^{-3}	0.213	0.0118	11.84	60.59	-87.46	10^{7}	0.20209	18.05

Table 2: Viscosity data for CPRI, CPRP and PENNZ lubricants from [27-28]

Finally, all numerical tests are carried out for Steel-Steel contacts. The employed Steel has a Poisson's coefficient $\upsilon=0.3$ and a Young's Modulus $E=210\text{GPa}$.

5.1 Convergence and Complexity

In this section, the convergence behavior of the proposed model with respect to the mesh size is studied along with the complexity of both the full and reduced models. In order to study the convergence behavior of the EHL solution with respect to the mesh size, two typical EHL cases are considered $M=30$, $L=5$ ($p_h=0.46\text{GPa}$) and $M=500$, $L=10$ ($p_h=3.78\text{GPa}$). The values of the dimensionless central film thickness H_c and minimum film thickness H_{min} (obtained by the full model) are reported in Figure 8 for the five different mesh cases considered.
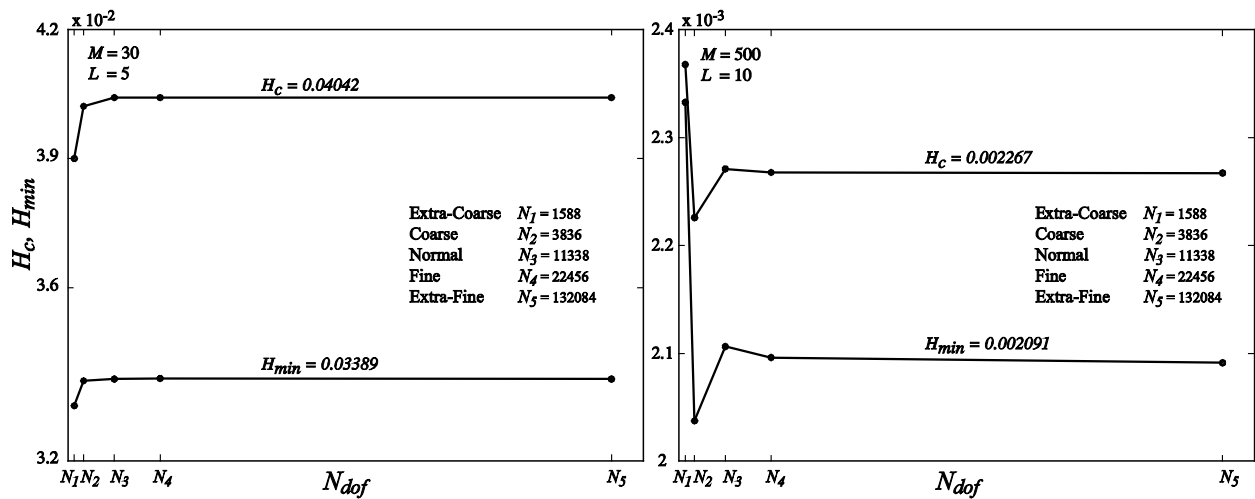
Figure 8: Solution convergence behavior of the proposed model with respect to the mesh size. Left: Lightly loaded case ($M=30$, $L=5$); Right: Highly loaded case ($M=500$, $L=10$)

Figure 8 (left) clearly shows that for the lightly loaded case ($M=30$, $L=5$) convergence of the central and minimum dimensionless film thicknesses is reached for the *"Normal"* mesh case. However, for the highly loaded case ($M=500$, $L=10$), convergence is reached for the *"Fine"* mesh case. This feature is common to all EHL models, since highly loaded contacts are known to

be more numerically sensitive to mesh size variations. Based on these results, from this point on, unless stated otherwise, the *"Fine"* mesh case is adopted for numerical tests.

Full Model		Reduced Model	
N_{dof}	Execution time / Newt. iter. (s)	$\tilde{N}_{dof}$	Execution time / Newt. iter. (s)
1588 (= n_{ref})	0.015(= t_{ref})	135 (= n_{ref})	0.004(= t_{ref})
3836	0.043	233	0.006
11338	0.135	529	0.015
22456	0.284	939	0.029
132284	2.017	4259	0.182

Table 3: Execution time for one Newton iteration as a function of the total number of dof for a typical line contact

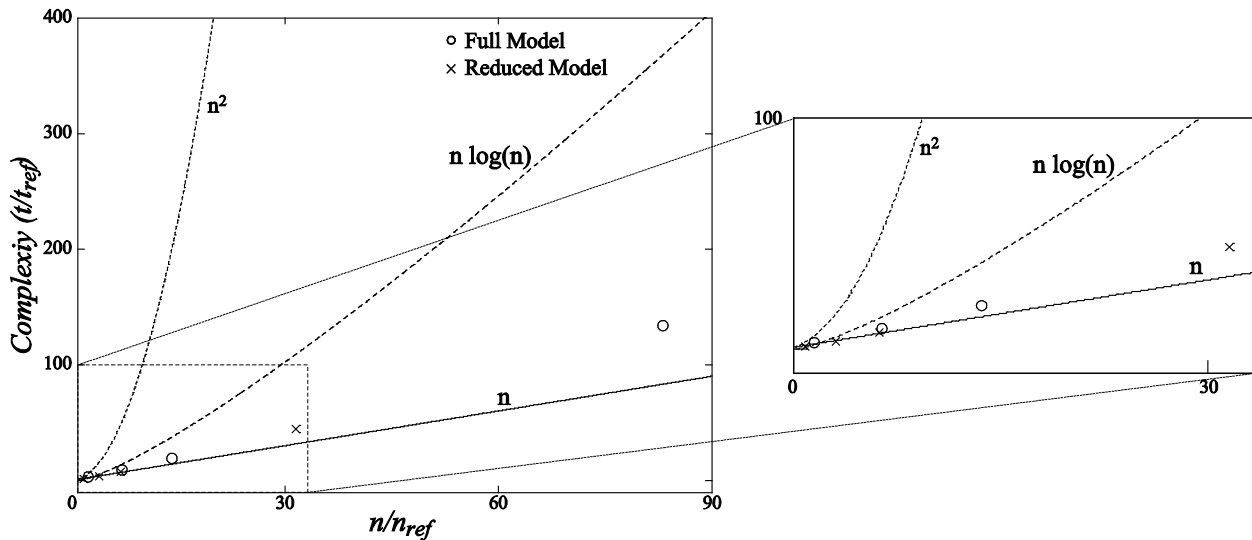(*M*=30, *L*=5) for both the full and reduced models

Figure 9: Experimental complexity of the proposed full and reduced models

Finally, the complexity of both the full and reduced models is studied. Table 3 lists the execution time required for one Newton iteration by both models (using a 2.4GHz processor) for a typical line contact case (*M*=30, *L*=5) as a function of the total number of dof. These results are used to plot the overall global complexity of the full and reduced model algorithms as shown in Figure 9. This figure shows the experimental complexity of the Full and Reduced models as compared to three reference complexities (n, $n \log(n)$ and n^2). From Figure 9, it is clear that both models have a complexity close to $O(n)$ over a wide range of the total number of dof ($n/n_{ref} < 30$). However,

as the total number of dof is further increased the complexity becomes slightly higher than $O(n)$ but remains below $O(n.log(n))$ or even more $O(n^2)$ over the considered range of n/n_{ref}. Note that the execution time per Newton iteration is used to derive the complexity curves. This is because the total execution time might be misleading as for the same test case the total number of iterations might be different for the Full and Reduced models since the stopping criterion for the damped-Newton procedure is error-based [20]. Hence, the execution time per iteration is more representative of the amount of computational effort required by each model for a given number of dof.

5.2 Reduced vs. Full Model

In this section, a series of numerical tests is realized in order to compare the precision and performance of the reduced model to that of the full one. The corresponding results are listed in Tables 4 and 5. All results discussed here are obtained using the "*Fine*" mesh case. Table 4 provides the dimensionless central film thickness H_c and minimum film thickness H_{min} obtained by both the full and reduced models for several test cases using the three different lubricants mentioned previously. Note that the errors reported in this table correspond to relative errors between the Full and Reduced models' respective solutions (where the Full model solution is used as the reference solution).

	M	L	p_h (GPA)	H_c Full	H_c Red.	Err.(‰)	H_{min} Full	H_{min} Red.	Err.(‰)
CPRI	12	12	0.70	0.18052049	0.18052302	0.014	0.15514818	0.15514674	0.009
	17	15	1.04	0.13772694	0.13771578	0.081	0.12093119	0.12083193	0.821
	45	5	0.57	0.02515687	0.02515679	0.003	0.02128733	0.02136252	3.532
	100	10	1.69	0.01438153	0.01438083	0.049	0.01290887	0.01291139	0.195
	600	8	3.31	0.00159831	0.00159830	0.006	0.00147220	0.00147069	1.026
CPRP	13	8	0.92	0.13077684	0.13074332	0.256	0.11272771	0.11259963	1.136
	40	9	1.82	0.03846414	0.03847607	0.310	0.03416566	0.03424579	2.345
	45	5	1.07	0.02465579	0.02458083	3.040	0.02129696	0.02142663	6.089
	120	10	3.50	0.01165195	0.01166741	1.327	0.01055419	0.01057317	1.798
	500	6	4.28	0.00166994	0.00167389	2.365	0.00153944	0.00154153	1.358
PENNZ	12	8	0.61	0.14334110	0.14334916	0.056	0.12171494	0.12156599	1.224
	18	15	1.41	0.12726978	0.12728937	0.154	0.11291462	0.11288638	0.250
	40	12	1.68	0.04516983	0.04519063	0.460	0.04031014	0.04036518	1.365
	200	12	3.75	0.00719969	0.00720202	0.324	0.00658494	0.00658984	0.744
	600	6	3.25	0.00133440	0.00133627	1.401	0.00122894	0.00123036	1.155

Table 4: Error behavior: comparison between the full and reduced models

Table 4 clearly shows that the relative error in H_c and H_{min} for the reduced model with respect to the full one is negligible. Despite the small number of basis functions employed, for most cases, the relative error is less than 1‰. Note that this is valid for all tested lubricants without the need to derive a new set of basis functions for each. Although, these lubricants have very different viscosities and viscosity-pressure dependencies, the choice of basis functions did not show any dependence on the choice of lubricant. In fact, for this work CPRI lubricant has been used when deriving the basis functions. This is probably why the deviations in film thickness between the reduced and full models is relatively lower than for the remaining lubricants considered here.

	M	L	p_h (GPA)	Nº of Iterations		Execution time (s)	
				Full	Red.	Full	Red.
CPRI	12	12	0.70	13	16	4.20	0.45
	17	15	1.04	23	38	7.60	1.10
	45	5	0.57	11	11	3.80	0.30
	100	10	1.69	17	17	5.40	0.68
	600	8	3.31	24	16	8.20	0.51
CPRP	13	8	0.92	14	14	4.70	0.38
	40	9	1.82	13	20	7.10	0.59
	45	5	1.07	8	10	2.90	0.28
	120	10	3.50	16	17	5.20	0.71
	500	6	4.28	27	25	10.0	0.99
PENNZ	12	8	0.61	14	16	4.60	0.44
	18	15	1.41	49	50	15.0	1.50
	40	12	1.68	27	29	8.40	0.86
	200	12	3.75	25	27	8.30	0.81
	600	6	3.25	30	24	11.0	1.00

Table 5: Performance analysis: comparison between the full and reduced models

Finally, Table 5 compares the performance of the reduced model to that of the full one in terms of convergence behavior (Nº of iterations required for convergence) and execution times for the test cases considered in Table 4. The results suggest that the convergence behaviors of both models are virtually identical. However, although the number of iterations is practically the same, in most cases the reduced model shows an order of magnitude execution time gain with respect to the full model. This is because of the smaller size systems obtained with the former. Finally, note the relatively small number of iterations required for a converged solution using this full-system damped-Newton approach. This clearly highlights the attractive feature of this type of approach as indicated previously.

Remark: The elastic deflections used to form the basis vectors of the EHL-basis were computed for a Steel-Steel contact. A different combination of solid materials would require the development of a new EHL-basis. However, in practice, for EHL applications, the number of possible combinations is very small and one can derive and store an EHL-basis for each possible

combination. This would require an additional effort during the preprocessing phase. But again, this is done only once for every solid material combination.

6. Conclusion

This paper presents a novel reduced model for a fast and robust solution of EHL problems. The developed approach is applied to the isothermal Newtonian line contact case, operating under steady-state regime. The model is based on a Full-System finite element resolution of the EHL equations: Reynolds, linear elasticity and load balance. A model reduction technique is derived to reduce the size of the linear elasticity problem. This leads to a significant reduction in the size of the global discrete system of equations, leading to a considerable reduction in execution time. The model is shown to be robust, allowing the solution of the EHL problem over a wide range of operating conditions. Its complexity is shown to be approximately $O(n)$. The relative error in the film thickness results for the reduced model compared to the full one is shown to be of the order of only 1‰ under a wide range of operating conditions.

Although the simple isothermal Newtonian line contact case is considered in this work, the developed approach can be extended to more general cases. In fact, this work aimed to prove the applicability of Model Order Reduction techniques to the elastic part of the EHL problem and demonstrate its attractive execution time reduction feature. The latter is of minor importance in the line contact case, since the corresponding solution can be obtained relatively fast even in the full model case. This feature would be of much greater importance for more computationally demanding applications (e.g. transient regime, point contacts). The extension of the reduced model to these cases is planned for future work.

Nomenclature

A_1, A_2 : Modified WLF model constant parameters

B_1, B_2 : Modified WLF model constant parameters

C_1, C_2 : Modified WLF model constant parameters

E_i : Young's modulus of solid body i

E_{eq} : Equivalent Young's modulus

F : External load

H : Dimensionless film thickness

H_0 : Dimensionless film thickness constant parameter

L : Dimensionless Moes material properties parameter

M : Dimensionless Moes load parameter

N_{1D} : Number of dof in the *1D* hydrodynamic problem

N_{2D} : Number of dof in the *2D* linear elasticity problem

N_{dof} : Total number of dof of the full model

$\tilde{N}_{dof}$: Total number of dof of the reduced model

N_m : Number of basis functions employed in the reduced model

P : Dimensionless pressure

Pe : Peclet number

R : Cylindrical roller radius

S_P : Pressure solution space

S_U : Elastic deflection solution space

$\tilde{S}_U$: Elastic deflection reduced solution space

T_0 : Ambient temperature

$T_g(0)$: Lubricant's ambient pressure glass transition temperature

X : Dimensionless space coordinate

a : Hertzian contact half-width

p : Pressure

p_h : Hertzian pressure

u_i : Surface velocity of solid body i

u_m : Mean entrainment speed

α^* : Equivalent pressure-viscosity coefficient

μ_g : Lubricant's viscosity at glass transition temperature

μ_R : Lubricant's reference viscosity

$\bar{\mu}$: Lubricant's dimensionless viscosity

v_i : Poisson's coefficient of solid body i

v_{eq} : Equivalent Poisson's coefficient

φ^i : Basis function i

$\bar{\rho}$: Lubricant's dimensionless density

ρ_R : Lubricant's reference density

Subscripts

e : Elastic

h : Hydrodynamic

l : Load balance

Dimensionless parameters

$$X = \frac{x}{a} \qquad P = \frac{p}{p_h} \qquad \bar{\rho} = \frac{\rho}{\rho_R} \qquad \bar{\mu} = \frac{\mu}{\mu_R} \qquad H = \frac{hR}{a^2}$$

References

[1]   Dowson D. and Higginson G. R. – A Numerical Solution of the Elastohydrodynamic Problem. *J. Mech. Eng. Sci.*, 1959, vol. 1, n° 1, pp. 6-15.

[2]   Hamrock B. J. and Dowson D. – Isothermal Elastohydrodynamic Lubrication of Contacts, Part I – Theoretical Formulation. *ASME J. of Lubr. Techn.*, 1976, vol. 98, n° 2, pp. 223-229

[3]   Lubrecht A.A., ten Napel W. E. and Bosma R. – Multigrid, an Alternative Method for Calculating Film Thickness and Pressure Profiles in Elastohydrodynamically Lubricated Line Contacts. *ASME, J. of Tribol.*, 1986, vol.108, pp. 551-556.

[4]   Rohde S. M. and Oh K. P. – A Unified Treatment of Thick and Thin Film Elastohydrodynamic Problems by Using Higher Order Element Methods. *Proc. Roy. Soc. London*, 1975, Part A, vol. 343, pp. 315-331.

[5]   Houpert L. G. and Hamrock B. J. – Fast Approach for Calculating Film Thicknesses and Pressures in Elastohydrodynamically Lubricated Contacts at High Loads. *ASME J. of Tribol.*, 1986, vol. 108, pp. 411-420.

[6]   Hughes T. G., Elcoate C. D. and Evans H. P. – Coupled Solution of the Elastohydrodynamic Line Contact Problem Using a Differential Deflection Method. *Proc. IMechE J. Mech. Engnrng. Sc.*, 2000, Part C, vol. 214, pp. 585-598.

[7]   Evans H. P. and Hughes T. G. – Evaluation of Deflection in Semi-Infinite Bodies by a Differential Method. *Proc. IMechE J. Mech. Engnrng. Sc.*, 2000, Part C, vol. 214, pp. 563-584.

[8]   Habchi W, Eyheramendy D, Vergne P and Morales-Espejel, G. A - Full-System Approach of the Elastohydrodynamic Line / Point Contact Problem. *ASME Journal of Tribology,* 2008; vol. 130 (2), DOI: 10.1115/1.2842246.

[9]   Habchi W. – A Full-System Finite Element Approach to Elastohydrodynamic Lubrication Problems: Application to Ultra-Low-Viscosity Fluids, *PhD Thesis,* 2008, INSA de Lyon, France.

[10]   Habchi W., Eyheramendy D., Vergne P. and Morales-Espejel G. – Stabilized Fully-Coupled Finite Elements for Elastohydrodynamic Lubrication Problems, *Advances in Engineering Software*, 2012, vol. 46, pp. 4-18.

[11]   Wu S. R. – A Penalty Formulation and Numerical Approximation of the Reynolds-Hertz Problem of Elastohydrodynamic Lubrication. *Int. J. Engnrng. Sci.*, 1986, vol. 24 (6), pp. 1001-1013.

[12]   Reynolds O. – On The Theory of the Lubrication and its Application to Mr Beauchamp Tower's Experiments, Including an Experimental Determination of the Viscosity of Olive Oil. *Phil. Trans. R. Soc.*, 1886, vol. 177, pp.157-234.

[13]   Ahmad S., Goodyer C. E. and Jimack P. K. – An Efficient Preconditioned Iterative Solution of Fully-Coupled Elastohydrodynamic Lubrication Problems, *Appl. Num. Math.*, 2012, vol. 62, pp. 649-663.

[14]   Brebbia C. A., Telles J. C. F. and Wrobel L. C. - Boundary Element Techniques. *Springer-Verlag*, Berlin, 1984.

[15]   Bettess P. – Infinite Elements. *Penshaw Press*, Cleadon, U.K., 1992.

[16]   Qu Z.Q. – Model Order Reduction Techniques with Applications in Finite Element Analysis. *Springer*, UK, 2004.

[17]   Hertz H. – Uber die Berührung fester Elastischer Körper. *J. reine und angew. Math.*, 1881, vol. 92, pp. 156-171.

[18]   Yasutomi S., Bair S. and Winer W. O. - An Application of a Free-Volume Model to Lubricant Rheology, (1) Dependence of Viscosity on Temperature and Pressure. *ASME J. of Tribol.*, 1984, vol. 106, pp. 291-312.

[19]   Dowson D. and Higginson G. R. – Elastohydrodynamic Lubrication. The Fundamental of Roller and Gear Lubrication. *Oxford, Pergamon* (1966).

[20]   Deuflhard P. – Newton Methods for Nonlinear Problems, Affine Invariance and Adaptive Algorithms. *Springer*, Germany, 2004.

[21]   Davis T. A. and Duff I. S. - An Unsymmetric-Pattern Multifrontal Method for Sparse LU Factorization, *SIAM Journal on Matrix Analysis and Applications*, vol. 18, no. 1, pp. 140-158, 1997.

[22]   Noor A. K. – Recent Advances and Applications of Reduction Methods. *Appl. Mech. Rev.,* vol. 47 (5), pp. 125-145, 1994.

[23]   Moes H. – Optimum Similarity Analysis with Applications to Elastohydrodynamic Lubrication. *Wear*, vol. 159, pp. 57-66, 1992.

[24]   Wilson E. L., Yuan M. W. and Dickens J. M. – Dynamic Analysis by Direct Superposition of Ritz Vectors. *Earthquake Engineering and Structural Dynamics,* vol. 10, pp. 813-821, 1982.

[25]   Nour-Omid B. and Clough R. W. – Dynamic Analysis of Structures using Lanczos Coordinates. *Earthquake Engineering and Structural Dynamics,* vol. 12, pp. 565-577, 1984.

[26]   Nour-Omid B. and Clough R. W. – Block Lanczos Method for Dynamic Analysis of Structures. *Earthquake Engineering and Structural Dynamics,* vol. 13, pp. 271-275, 1985.

[27]   S. Bair – Reference Liquids for Quantitative Elastohydrodynamics: Selection and Rheological Characterization, Tribology letters, vol. 22, no 2, pp. 197-206, May 2006.

[28]   Molimard J., Querry M. and Vergne P. – Rhéologie du Lubrifiant en Conditions Réelles: Mesures et Confrontation à un Contact Bille-Plan. *La Revue de Métallurgie,* CIT/Science et Génie des Matériaux, pp. 141-148, February 2001.

[29]   Nélias D., Legrand E., Vergne P. and Mondier J. B. – Traction Behaviour of Some Lubricants Used for Rolling Bearings in Spacecraft Applications: Experiments and Thermal Model Based on Primary Laboratory Data. *ASME Journal of Tribology,* vol. 124, pp. 72-81, 2002.